



HAL
open science

Late Pleistocene to Holocene tephrostratigraphic record from the Northern Ionian Sea

Benoît Caron, G Siani, R Sulpizio, G Zanchetta, M Paterne, R Santacroce, E Tema,
E Zanella

► **To cite this version:**

Benoît Caron, G Siani, R Sulpizio, G Zanchetta, M Paterne, et al.. Late Pleistocene to Holocene tephrostratigraphic record from the Northern Ionian Sea. *Marine Geology*, 2012, 311-314, pp.41 - 51. <10.1016/j.margeo.2012.04.001>. <hal-03634466>

HAL Id: hal-03634466

<https://hal.science/hal-03634466v1>

Submitted on 11 Apr 2022

HAL is a multi-disciplinary open access archive for the deposit and dissemination of scientific research documents, whether they are published or not. The documents may come from teaching and research institutions in France or abroad, or from public or private research centers.

L'archive ouverte pluridisciplinaire **HAL**, est destinée au dépôt et à la diffusion de documents scientifiques de niveau recherche, publiés ou non, émanant des établissements d'enseignement et de recherche français ou étrangers, des laboratoires publics ou privés.



HAL Authorization

Marine Geology
Manuscript Draft

Manuscript Number: MARGO4600

Title: Late Pleistocene to Holocene tephrostratigraphic record from the Northern Ionian Sea.

Article Type: Research Paper

Keywords: Tephrochronology, Ionian Sea, Somma-Vesuvius, Mercato, Lipari, Gabelotto-Fiumebianco/E-1, Monte Pilato, Monte Guardia, volcano, Italy

Highlights

8 tephra layers are present across the last 20 ka in the marine core MD90-918. > Most of these tephra are derived from Somma-Vesuvius and Aeolian Islands. > We provide new clues about the volcanic activity from Lipari and Somma-Vesuvius. > Results provide new data of ash dispersal from Lipari and Somma-Vesuvius volcanoes. > Mercato tephra layer is a powerful time marker for the onset of Sapropel S1a interval

1 Late Pleistocene to Holocene tephrostratigraphic record from the Northern
2 Ionian Sea.

3
4
5 Caron B.^{1,2,*}, Siani G.¹, Sulpizio R.^{3,4}, Zanchetta G.^{2,5,6},
6 Paternò M.⁷, Santacroce R.², Tema E.^{8,9}, Zanella E.^{8,9}

7
8
9 ¹*Laboratoire des Interactions et Dynamique des Environnements de Surface (IDES), UMR*
10 *8148, CNRS-Université de Paris-Sud, Bât 504, 91405 Orsay Cedex, France*

11 ²*Dipartimento di Scienze della Terra, Via S. Maria 53, 56126 Pisa, Italy*

12 ³*CIRISIVU, c/o Dipartimento Geomineralogico, via Orabona 4, 70125, Bari, Italy*

13 ⁴*IDPA-CNR, via Mario Bianco 9, 20131, Milano, Italy*

14 ⁵*IGG-CNR Via Moruzzi, 1, 56100, Pisa, Italy*

15 ⁶*INGV-Pisa, Via della Faggiola, 32, 56126 Pisa, Italy*

16 ⁷*Laboratoire des Sciences du Climat et de l'Environnement, Laboratoire Mixte CNRS-CEA -*
17 *UVSQ, Avenue de la Terrasse 91198 Gif-sur-Yvette Cedex, France*

18 ⁸*Dipartimento di Scienze della Terra, Via Valperga Caluso 35, 10125 Torino, Italy*

19 ⁹*ALP, Alpine Laboratory of Paleomagnetism, 12016 Peveragno, Italy*

20 * *Present address UFR TEB 918, Université Pierre et Marie Curie, 4 place Jussieu, 75005 Paris*

21
22
23
24 *Corresponding author:

25 Université Pierre et Marie Curie, UPMC, UFR TEB 918

26 Benoît Caron : benoit.caron@upmc.fr

27 + 33 (0)1 44 27 73 86

28 ABSTRACT

29
30 A detailed tephrostratigraphic study supported by stable isotope ($\delta^{18}\text{O}$) analyses and AMS ^{14}C
31 dating was carried out on a high sedimentation rate deep-sea core recovered in the northern
32 Ionian Sea. Eight tephra layers were recognized, all originated from explosive eruptions of
33 southern Italian volcanoes. These tephra layers are correlated with terrestrial proximal
34 counterparts and with both marine and lacustrine tephra already known in the central
35 Mediterranean area. The oldest tephra (dated at ca. 19.4 ka cal BP) is tentatively correlated to
36 the Monte Guardia eruption from Lipari Island. Two other rhyolitic tephra layers were
37 correlated with the explosive volcanic activity of Lipari Island: Gabelotto-Fiumebianco/E-1
38 (8.3 ka cal BP) located close to the interruption of Sapropel S1 deposit, and Monte Pilato (ca.
39 AD 1335) in the uppermost part of the core. The Na-phonolitic composition of the other five
40 recognized tephra layers indicates the Somma-Vesuvius as the source. The composition is
41 quite homogeneous among the five tephra layers, and fits that of the Mercato proximal
42 deposits. Beyond the striking chemical similarity with the Mercato eruption, these tephra
43 layers spans over ca. 2000 years, preventing correlation with the single well known Plinian
44 eruption of the Somma-Vesuvius. Therefore, at least two of these tephra layers were assigned
45 to an interplinian activity of the Somma-Vesuvius between the eruptions of Mercato and
46 Avellino, even though these eruptions remains poorly constrained in the proximal area. By
47 contrast, the most prominent tephra layer (2 mm white tephra visible at naked eyes) was
48 found within the S1a Sapropel interval. Despite the possible complication for the presence of
49 similar eruption with different ages we argue that Mercato is probably a very good marker for
50 the onset of sapropelic condition in the Ionian Sea and can be used for land-sea correlations
51 for this important climatic event. More in general, these data allow a significant update of the
52 knowledge of the volcanic ash dispersal from Lipari and Somma-Vesuvius volcanoes.

53

54 *Keywords:* tephrochronology, Ionian Sea, Somma-Vesuvius, Mercato, Lipari, Gabelotto-
55 Fiumebianco/E-1, Monte Pilato, Monte Guardia, volcano, Italy

56

57

58 **1. Introduction**

59

60 The central Mediterranean region represents one of the most suitable area for
61 tephrostratigraphic studies across the Quaternary as displayed through early studies by Keller
62 et al. (1978), Thunell et al. (1979), McCoy (1981) and Paterne et al. (1986). Significantly,
63 over the last decades, marine tephra studies in this area have allowed to improve the
64 reconstruction of the explosive activity of the Mediterranean volcanoes (e.g. Keller et al.,
65 1978; Paterne et al., 1986, 1988, 1990, 2008; Siani et al., 2004; Lowe et al., 2007; Margari et
66 al., 2007; Turney et al., 2008; Bourne et al., 2010). In addition to their interest for
67 volcanology, the identification of tephra layers on land and/or in the marine sediments have
68 supplied a significant stratigraphic support to paleoclimatic and paleoceanographic
69 investigations in this basin, improving chronology and correlation of marine, continental, and
70 cryospheric records at ultra-regional scale (e.g. Paterne et al. 1986; Siani et al., 2001; Lane et
71 al., 2010; Zanchetta et al., 2011).

72 The Tyrrhenian, Adriatic and Ionian seas are the best studied basins of the
73 Mediterranean because of the prevailing seasonal wind directions that mainly dispersed ash
74 particles to the east and southeast, at least for the last 200 ka (Keller et al., 1978; Paterne et
75 al., 1990, 2008; Siani et al., 2004; Bourne et al., 2010). However, the inspection of the
76 location of the published cores shows an evident lack of data in the north part of the Ionian
77 Sea. This creates a gap in the tephrostratigraphic network among the different marine basins
78 and continental archives. In order to fill this gap, we selected a high sediment accumulation
79 rate deep-sea core located in the northern Ionian Sea (MD 90-918; Fig. 1) for detailed
80 tephrostratigraphic studies. The ages of the marine tephra have been obtained through

81 accelerator mass spectrometry (AMS) ^{14}C dating coupled to oxygen isotope measurements
82 performed on monospecific planktonic foraminifera. The origin of the tephra layers were
83 assessed by comparing major element compositions (SEM-EDS analyses), age estimates and
84 morphological characteristics of vitric fragments with those of corresponding subaerial
85 pyroclastic deposits. Here, an evaluation and refinement of the dispersal areas of some of the
86 recognized eruptions is presented, in view to providing a contribution for the improvement of
87 volcanic hazard assessment in the central Mediterranean area.

88

89 **2. Material and analytical methods**

90

91 *2.1. Core lithology*

92 Core MD 90-918 was recovered in the northern Ionian Sea (39° 35,64 N, 18°5 0,43 E;
93 695 m water depth, 14.77 m core length; Fig. 1) during the 1990 PROMETE II cruise of the
94 French N/O Marion Dufresne. Grey hemipelagic ooze dominates the core lithology except for
95 a 20 cm thick sandy layer centred at 992 cm depth representing a turbidite deposit (Fig. 2). A
96 black-grey layer in the upper part of the core (between 204 and 231 cm depth), is referred to
97 the Sapropel S1 deposit. This layer was deposited during the most recent period of stagnation
98 in the East Mediterranean Sea (e.g. Kallel et al., 1997; Rohling et al., 1997, Mercone et al.,
99 2000) and is marked by two black-grey beds (i.e. S1a and S1b) separated by a thin horizon of
100 white hemipelagic ooze between 210 and 219 cm depth (Fig. 2).

101

102 *2.2 Detection and chemical analysis of tephra*

103 Core MD 90-918 was sampled at 5 cm interval for recognition of volcanic particles for
104 its entire length, with the exception of the Sapropel S1 deposit (between 204 and 231 cm) that
105 was sampled at 1 cm interval. Each sample was then washed and sieved in the fraction > 40
106 μm . Tephra layers are then defined by the relative abundance of volcanic glass shards with

107 respect to detrital crystals and lithics in the same fraction after counting of at least 400
108 particles under a stereo-microscope. Volcanic glass occurs throughout the core, and forms a
109 background at about 4 % of abundance for the 323 counted samples (Fig. 2). Therefore, we
110 considered only abundance peaks larger than two times the background as representative of
111 tephra deposition and selected for laboratory analyses. Glass shards and/or micropumice
112 fragments were morphologically and lithologically described under stereo-microscope, then
113 hand-picked and mounted on epoxy resin beads and polished in order to avoid compositional
114 variations due to surface alteration processes.

115 Two different facilities were used to analyse the major element composition of micropumices
116 and/or glass shards: the CAMECA-SX 100 Electron Probe Micro-Analyser (EPMA-
117 CAMPARIS) available at the University Pierre et Marie Curie – Paris 6 (France) and the
118 Philips SEM 515 device equipped with an EDAX-DX micro-analyser (SEM-DST) available
119 at Dipartimento di Scienze della Terra (University of Pisa, Italy). Working conditions of
120 EPMA-CAMPARIS comprise an acceleration voltage of 15 kV and a beam current of 4 nA.
121 Usually, analytical data show closures > 97 wt. %, which indicate a limited or absent
122 alteration of analysed glasses. Working conditions of SEM-DST were 20 kV acceleration
123 voltage, 100 s live time counting, 1 nA beam current, 20-10 µm beam diameter, 2100 shots
124 per second, ZAF correction. The ZAF correction procedure does not include natural or
125 synthetic standards for reference, and requires the analyses normalization at a given value
126 (which is chosen at 100 %).

127 The variance of analytical precision between the two instruments was calculated using the
128 mean of the analyses from 5 tephra layers recognized along the core. The analysis indicates
129 that the difference in composition of the different tephra layers has not incidence on the
130 variance between both instruments. The variance of the SEM relatively to the EPMA is
131 reported in Table 1. Variance was not calculated for the P₂O₅, which is under the detection

132 limit of the EDS analyses. The intercalibration shows the full comparability of the EPMA-
133 CAMPARIS and SEM-DST. The different tephra layers were classified using the Total Alkali
134 vs. Silica diagram (TAS, Le Bas et al., 1986; Fig. 3).

135

136 *2.3 Stable isotope analysis*

137 Oxygen isotope measurements were obtained on the planktonic foraminifera
138 *Globigerinoides ruber* (250-315 μm) with a sampling resolution every 10 cm. Between 6 to
139 10 shells were picked and then cleaned in a methanol ultrasonic bath for few seconds then
140 roasted under vacuum at 380°C for 45 minutes, prior to isotopic analyses. Isotopic
141 composition was expressed in δ -‰ unit and normalized to the Vienna Pee Dee Belemnite
142 scale (V-PDB) using the international standards NBS18. Analyses were performed at the
143 Laboratoire des Sciences du Climat et de l'Environnement (LSCE, Gif-sur-Yvette, France)
144 using a Finnigan Delta Plus mass-spectrometers. The mean external reproducibility (1σ) of
145 carbonate standards (NBS18 $\delta^{18}\text{O} = -23.2 \pm 0.1\text{‰}$) was $\pm 0.05\text{‰}$.

146

147 *2.4 Radiocarbon dating*

148 Radiocarbon analyses were performed by UMS-ARTEMIS (Pelletron 3MV) AMS
149 facilities (CNRS-CEA Saclay, France) on monospecific planktonic foraminifera in the size
150 fraction $>150 \mu\text{m}$ (Table 2). To minimize the effect of bioturbation, the sampling was limited
151 to peaks of maximum abundance of planktonic foraminifera (Bard et al., 1987). The
152 conventional radiocarbon ages were subsequently converted into calendar ages, based on
153 INTCAL09 (Reimer et al., 2009) using the ^{14}C calibration software CALIB 6 (Stuiver et al.,
154 1998). The calibration integrate a marine reservoir correction $R(t)$ of about 400 years (Siani et
155 al., 2000).

156

157 2.5 Rock magnetic properties

158 A total of 539 samples were collected at ca. 3 cm interval along the total core length,
159 using plastic cubic boxes of standard size (2 cm of length). Measurements were carried out at
160 the ALP palaeomagnetic laboratory (Peveragno, Italy). Magnetic susceptibility (k), natural
161 remnant magnetization (NRM) and NRM demagnetized in alternating field (AF) at 25 mT
162 peak-field (NRM₂₅) were measured using a KLY-3 kappabridge and a 2G cryogenic
163 magnetometer respectively. After completion of all measurements, the samples were dried
164 and weighted in order to normalize the magnetic parameters by the mass. The mean water
165 content was in the order of 40-50%.

166

167 3. Results

168

169 3.1 Age model

170 The stratigraphy of core MD 90-918 was derived from the $\delta^{18}\text{O}$ variations of the
171 planktic foraminifera *Globigerinoides ruber* (Fig. 2). The $\delta^{18}\text{O}$ values range between 3.5 to -
172 0.3 ‰ exhibiting a pattern similar to those observed in nearby south Adriatic deep-sea cores
173 (Fontugne et al., 1989; Siani et al. 2001, 2010). The late glacial, the last glacial/interglacial
174 transition and the Holocene encompass the upper 1470 cm of the core, leading to a highly
175 detailed record of both the two-steps of the deglaciation marked by two abrupt shifts toward
176 depleted $\delta^{18}\text{O}$ values from 590 cm to 430 cm and from 300 cm to 230 cm (Termination IA
177 and IB; Duplessy et al., 1981; Bard et al., 1987) and the Holocene.

178 The age model of the core MD 90-918 was then based on 7 AMS ^{14}C measurements
179 performed on monospecific planktonic foraminifera in the size fraction $>150\mu\text{m}$ (Table 2), by
180 a linear interpolation of two consecutive ages. In addition, comparison of the oxygen isotope
181 record with that of the South Adriatic Sea core MD 90-917 previously dated by several AMS

182 ^{14}C ages (Siani et al., 2001; 2010) provides three more age control points at 300 cm, 420 cm,
183 and 590 cm. Combination of the age points resulting from the two times series provides a
184 consistent age model covering the last 27.4 cal ka BP (Fig. 2). The calculated sedimentation
185 rate is estimated between ca. 30 cm/ka (from the top to 470 cm depth), for the last
186 glacial/interglacial transition to Holocene section and ca. 90 cm/ka during the late Glacial
187 (Fig. 2).

188

189 *3.2 Rock-magnetism*

190 Down-core mass susceptibility is shown in Figure 2. Mass susceptibility shows rather
191 uniform values along the core. As a whole, results indicate little fluctuations of the magnetic
192 mineralogy, both in magnetic grain concentration and mineral type. The lower values between
193 204 to 231 cm depth correspond to the S1 Sapropel interval. Four distinct spikes occur at
194 73.5, 771, 887 and 982 cm. The 982 cm spike could be correlated to a turbiditic sandy layer,
195 whereas the other three do not match evidences of lithological changes. No one of the tephra
196 layers found in the core match a distinctive change in the magnetic properties. This is
197 probably due to both their small thickness and high content in glass and micropumice. This
198 justify the glass-shard counting procedure used for tephra identification.

199

200 *3.3 Composition and origin of tephra layers*

201 The geochemical composition and the morphological characteristic of vitric fragments
202 are here presented for determining the proximal counterparts and the origins of the marine
203 tephra layers (Figs. 3, 4 and 5). One tephra and seven cryptotephra layers were recognized
204 along the core MD 90-918 and centred at 2, 175, 185, 210, 218, 223, 230 and 820 cm
205 respectively spanning the last 27.4 cal ka BP (Fig. 2). In particular, tephra layers between 210
206 and 230 cm form a cluster with high abundance of volcanic glass-shards (Fig. 4). Only the

207 peak at 223 cm is visible at naked eye inspection, while the other peaks were identified
208 through the high resolution counting of glass shards.

209

210 The cryptotephra centred at **2 cm** was dated at 0.6 cal ka BP (ca. AD 1335, Table 2)
211 and presents a homogeneous rhyolitic composition (Fig. 3; Table 3). It contains glass shards
212 with a glassy groundmass (Fig. 5a), and mean grain size coarser than 100 µm. The vesicles
213 are elongated to form fibrous glass shards.

214 The cryptotephra at **175 cm** and **185 cm** are dated at 7 and 7.3 cal ka BP, respectively
215 (Table 2). Both tephra present a homogeneous Na-phonolitic composition (Fig. 6b; Table 3)
216 and are equally characterised by highly vesicular, aphyric, white micropumices with a grain
217 size finer than 100 µm, and a glassy groundmass (Figs. 5b and c). The only difference
218 concerns the major elements analyses of the tephra at 185 cm showing a double Na-phonolitic
219 composition, with slight differences in CaO, Na₂O, K₂O and SiO₂ contents (Table 3).

220 The cryptotephra at **210 cm** presents a high glass abundance (Fig. 2). Inspection under
221 stereo-microscope shows that ca. 90 % of the volcanic glass are white micropumice and the
222 other 10 % glass shards (Fig. 4). Micropumice fragments are highly vesicular and aphyric,
223 with a glassy groundmass with grain size finer than 100 µm. The second ones are small
224 rounded bubbles and aphyric, glassy groundmass with grain size finer than 50 µm (Fig. 5d).
225 The composition of micropumice fragments is homogeneous Na-phonolitic (Fig. 6b; Table 3),
226 very similar to the cryptotephra at 175 and 185 cm and present an interpolated age at ca. 8.1
227 cal ka BP. On the other hand, few glass shards show a homogeneous rhyolitic composition
228 (Fig. 6c; Table 3) representing the tails of the following tephra layer centred at **218 cm** (Fig.
229 4). This cryptotephra spreads between 216 and 219 cm and was deposited during the Sapropel
230 S1 interruption. It presents a homogeneous rhyolitic composition and an age of 8.3 cal ka BP

231 (Fig. 6c; Tables 2 and 3). This cryptotephra contains aphyric glass shards with small rounded
232 bubbles and a mean grain size finer than 50 μm (Fig. 5e).

233 The tephra layer at **223 cm** is visible at naked eye, and contains exclusively highly-
234 vesicular micro-pumices with rounded bubbles and a glassy groundmass (Fig. 5f). The glass
235 composition is Na-phonolitic ($\text{K}_2\text{O}/\text{Na}_2\text{O}$ lower than 1) with high Al_2O_3 content (Fig. 6b;
236 Table 3), and is similar to those of the cryptotephra at 175, 185 and 210 cm. The interpolated
237 age is of ca. 8.6 cal ka BP.

238 The cryptotephra at **230 cm** comprises white, aphyric and highly vesicular micro-
239 pumice with a glassy groundmass and a mean grain size around 50 μm (Fig. 5g). The glass-
240 shards have a Na-phonolitic composition, with high Al_2O_3 content (Fig. 6b; Table 3), and is
241 similar to the previous cryptotephra at 175, 185, 210 and 223 cm. Calibrated radiocarbon
242 dating for this tephra layer gives an age of 9 cal ka BP (Table 2).

243 The last cryptotephra was recovered at **820 cm** and dated at 19.4 cal ka BP (Table 2).
244 It is composed of glass shards coarser than 100 μm (Fig. 5h) with a glassy groundmass and
245 rounded bubbles. The composition straddles between the trachytic and the rhyolitic fields
246 (Fig. 6d; Table 3).

247

248

249 **4. Discussion**

250 The available AMS ^{14}C ages and oxygen isotope stratigraphy indicate that the deep-
251 sea core MD 90-918 covers the late Pleistocene to Holocene period (i.e. the last 27.4 cal ka
252 BP). This constrains the search for the source of the parent eruptions of marine cryptotephra
253 and tephra layers to the explosive activity of Mediterranean volcanoes during this time
254 interval.

255 The recognized cryptotephra and tephra layers show alkaline and calc-alkaline affinity
256 (Fig. 3). The alkaline samples have mildly undersaturated glass compositions with alkali ratio
257 around or below 1 (Na-phonolites; Fig. 3; Table 3), and are younger than 9 ka (Fig. 2). The
258 composition and geochemical affinity limit their sources to Italian volcanoes, since the
259 sources in the Aegean area during the Holocene present a calc-alkaline affinity (e.g. Keller et
260 al., 1978). Sources from Massif Central (France) and Anatolia (Turkey, eastern
261 Mediterranean) can be rejected, though both volcanisms present K-alkaline affinity (Juvigné,
262 1987; Druitt et al., 1995), because their relatively low dispersion for the former and the
263 upwind location of the study core with respect to the Anatolian volcanoes (e.g. Zanchetta et
264 al., 2011).

265 The only Holocene source of K-alkaline, undersaturated magmas in the Mediterranean area is
266 Somma-Vesuvius (Santacroce et al., 2008), representing the inferred source for cryptotephra
267 at 175, 185, 210, 230 cm and the tephra layer at 223 cm. The geochemistry of Holocene
268 explosive products of Somma-Vesuvius (Santacroce et al., 2008) shows that Na-phonolitic
269 magmas fed the eruptions of the Pomici di Mercato (Santacroce, 1987; Aulinas et al., 2008;
270 Mele et al., 2010), and the initial stages of the Pomici di Avellino (ca. 3.8 ka BP, Sulpizio et
271 al., 2008, 2010). Because the Pomici di Mercato and the Pomici di Avellino (white pumice)
272 products show very different crystal content (almost aphyric vs. porphyritic; Aulinas et al.,
273 2008; Santacroce et al., 2008; Mele et al., 2010; Sulpizio et al., 2010), the glassy, aphyric, Na-
274 phonolitic micropumice and glass shards of the MD 90-918 core can be confidently correlated
275 to the Pomici di Mercato eruption (ca. 8.5 cal ka BP; Zanchetta et al., 2011).

276 Nevertheless, the attribution to the Pomici di Mercato eruption poses some problems in layer
277 by layer correlation of the Na-phonolitic cryptotephra and tephra layer to the proximal
278 stratigraphy of Somma-Vesuvius. The tephrostratigraphy of core MD 90-918 indicates 5
279 distinct depositional events over a time span of ca. 2000 years. On the basis of this

280 chronology, the correlation to a single eruption is unlikely, although the Mercato eruption was
281 recently described as a long lasting with a succession of pulsating event (Mele et al., 2010).
282 Based on field evidences, a reasonable duration of the Mercato eruption can be assessed at
283 some decades at maximum, but in any case neither to centuries nor to millennia.

284 The chronology of the Pomici di Mercato eruption spans from a maximum age of 9 cal ka BP
285 (Wulf et al., 2004) to 8.5 cal ka BP (Zanchetta et al., 2011). These ages are in fairly good
286 agreement with that reported in Delibrias et al. (1979), which provided a calibrated age at ca.
287 9.1 ka BP (paleosol under the Pomici di Mercato deposits, PSV 112 and PSV 113 samples).
288 This age range is in agreement with dating of both **230 cm** cryptotephra (9 cal ka BP) and **223**
289 **cm** tephra (interpolated age of 8.6 cal ka BP) layers, making it difficult to precisely
290 individuate the onset of the Pomici di Mercato eruption in core MD 90-918. In particular, it is
291 difficult to discriminate if the cryptotephra at 230 cm represents the first eruptive phase of the
292 Pomici di Mercato eruption or a small event preceding the main eruption and unknown in
293 proximal areas, since the deposits between the Greenish and Mercato eruptions (e.g.
294 Santacroce et al., 2008) show homogeneous K-trachytic composition (e.g. GM1; Zanchetta et
295 al., 2000; Siani et al., 2004).

296 The cryptotephra at **210 cm** is about 500 years younger (interpolated age of 8.1 ka) than the
297 tephra layer at 223 cm. Because it occurs within few centuries from the preceding tephra
298 layer, a correlation to the latest stages of the Mercato eruption is still possible. In particular, it
299 may be correlated to the Phase III of the eruption (Mele et al., 2010; previously known as
300 Pomici and Proietti; Santacroce, 1987), which is separated by the preceding Phase II by
301 erosion surfaces indicating volcanic quiescence between them.

302 A distinct discussion requires the origin of the cryptotephra at **175 and 185 cm**. Their
303 radiocarbon ages are significantly younger (between 7 and 7.3 cal ka BP) than the proximal
304 Pomici di Mercato deposits (8.5 cal ka BP), so their correlation to this eruption still remains

305 problematic. Firstly, stratigraphy, sedimentology, rock magnetic data and chronology exclude
306 extensive reworking of the sediment core. On the other hand, the two cryptotephra at 175 and
307 185 cm do not correspond to a distal counter part of known activity between the eruptions of
308 Mercato and Avellino, of the well-known Somma-Vesuvius stratigraphy (e.g. Santacroce and
309 Sbrana, 2003; Cioni et al., 2008; Santacroce et al., 2008). However, tephrostratigraphy study
310 from Holocene lake sediments of the Sulmona basin indicates the occurrence of numerous
311 tephra layers, recovered between Pomici di Mercato and Avellino eruptions, which do not
312 display any correlations with proximal deposits of Italian volcanoes (Giaccio et al., 2009).
313 Nevertheless, the occurrence of subplinian events between Pomici di Mercato and Avellino
314 eruption was reported by Delibrias et al., (1979) and chronologically constrained between two
315 paleosols dated at 8.6 and 6.3 cal ka BP (Alessio et al., 1974; Delibrias et al., 1979). The
316 origin of these Mercato-Avellino cryptotephra (MA group) remains enigmatic, and we cannot
317 rule out they could represent distal evidence of unknown Vesuvian activity.

318 Tephra layers compositionally similar to the Pomici di Mercato deposits were found in
319 lacustrine (TM6b in the Lago Grande di Monticchio; Wulf et al., 2004, 2008; OT02-3 in Lake
320 Ohrid; Vogel et al., 2010), and marine (KET 8218, Adriatic Sea; Paterne et al., 1988) cores
321 (Table 4). The recognition in core MD 90-918 enlarges the dispersal ash area of the Mercato
322 products to the southeast with an estimated geographical distribution at ca. 250,000 km² (Fig.
323 7).

324

325 Homogeneous rhyolitic cryptotephra with calc-alkaline affinity occur between **2 and 5**
326 **cm** and between **216 and 219 cm**. The available AMS ¹⁴C age measurements constrain the
327 former interval at ca. 0.6 cal ka BP, and the latter at ca 8.3 cal ka BP (Table 2). During this
328 period, calc-alkaline tephra were generated by explosive activity of both Aegean arc (Greece,
329 eastern Mediterranean) and Aeolian Islands volcanoes (southern Tyrrhenian Sea, central

330 Mediterranean). The evolved magmas from these two sources are hardly distinguishable
331 considering major and trace elements (Clift and Blusztajn, 1999). However, a source in the
332 Aegean Sea is unlikely taking into account the prevailing winds in the area, which
333 preferentially blow from west to east (Barberi et al., 1990; Costa et al., 2009; Folch and
334 Sulpizio, 2010). Therefore, an Aeolian Island origin is here assumed.

335 The rhyolitic tephra layer at the top of the core (**2-5 cm**; Fig. 2) is dated at ca. 0.6 cal ka BP
336 (AD 1321 – 1349; Table 2). Age and composition suggest a correlation to the eruption of
337 Monte Pilato from Lipari Island (Fig. 6a; Table 4), recently dated by archaeomagnetic
338 techniques between AD 1030-1528 (Zanella, 2006) or AD 1200-1240 (Arrighi et al., 2006).
339 This is the first recognition of Monte Pilato tephra in deep-sea cores of the Ionian Sea, and
340 enlarges the dispersal of this tephra to the East (Fig. 7).

341 The composition and the stratigraphy of the cryptotephra between **216 and 219 cm** matches
342 well that of the rhyolitic tephra layer E-1 (Paterne et al., 1988; Fontugne et al., 1989; Fig. 6c;
343 Table 4), which is correlated to the eruption of Gabelotto-Fiumebianco from Lipari Island
344 (Siani et al., 2004; Zanchetta et al., 2011). Siani et al. (2004) dated this eruption at 8.4 cal ka
345 BP through ¹⁴C AMS measurements on planktic foraminifera, an age in good agreement with
346 that of the 216-219 cryptotephra in core MD 90-918, dated at 8.3 cal ka BP. The recognition
347 of Gabelotto-Fiumebianco/E-1 tephra layers in core MD 90-918 enlarges its dispersal area to
348 the east (Fig. 7). The surface of the dispersal ash area can now be estimated at ca. 300,000
349 km². Moreover, it is interesting to point out that E-1 tephra recovered in cores MD 90-918 and
350 MD 90-917 presents a similar stratigraphic position between the end of the Sapropel S1a
351 interval and the Sapropel interruption.

352 The cryptotephra at **820 cm** is trachy-rhyolitic in composition, and is dated at 19.4 cal
353 ka BP (Table 2). These findings allow to correlate this tephra to the eruption of Monte
354 Guardia from Lipari Island. This is mainly because, among the known eruptions with trachy-

355 rhyolitic composition occurred around 20 cal ka BP like those of the Lower Pollara (Salina
356 Island, 24 cal ka BP; Calanchi et al., 1993), the Lentia cycle (Vulcano Island, 15-25 cal ka
357 BP; De Astis et al., 1997), and the third and fourth cycles from Pantelleria Island (Civetta et
358 al., 1988), it shows the best geochemical match (Fig. 6d; Table 4). In particular, the **820 cm**
359 tephra can be correlated to the less evolved component of the Monte Guardia eruption (MG4
360 base B sample; Table 4), which is characterised by an important geochemical variability due
361 to pre- and sin-eruptive processes of magma mixing and mingling (De Rosa et al., 2003). The
362 Monte Guardia eruption from Lipari Island has an age comprised between 22.4 ± 1.1 cal ka
363 BP and 20.3 ± 0.7 cal ka BP (Crisci et al., 1981, 1991; De Rosa and Sheridan, 1983), which is
364 in fairly good agreement with that obtained for the cryptotephra at **820 cm**.

365 The evolved products of the Monte Guardia eruption were also recognized in the sediments of
366 the Lago di Pergusa (central Sicily; Fig. 1; Narcisi, 2002), suggesting different dispersal areas
367 for ash produced at different times during the eruption. The first time recognition of Monte
368 Guardia tephra in the Ionian Sea sediments enlarges the dispersal area to the East (Fig. 7).

369

370 **5. Concluding remarks**

371

372 Seven cryptotephra and one tephra layer were identified in core MD 90-918: five of them are
373 correlated to Somma-Vesuvius and three to Lipari Island (Aeolian archipelago) volcanoes.

374 Tephra layers from Somma-Vesuvius are compositionally homogeneous Na-phonolites, and
375 are correlated to the Mercato eruption. Among them, only the tephra layer at 223 cm and the
376 cryptotephra at 210 cm are related to primary tephra deposition from a pyroclastic cloud,
377 while the depositional processes of the other three still remain puzzling. In particular, the two
378 upper Na-phonolitic cryptotephra are too young to be correlated to the Mercato eruption.
379 They may represent an interplinian activity occurred between the Mercato and Avellino

380 Plinian eruptions (MA group), though proximal counterparts are not described in the Somma-
381 Vesuvius stratigraphy. However, new tephrochronology studies from distal archives are
382 needed to confirm the presence of this activity. The tephra layer at 223 cm occurs within the
383 Sapropel S1, confirming the Mercato eruption as a good marker for the Sapropel S1a interval.
384 Cryptotephra from Lipari Island are all rhyolitic, and are correlated to Monte Pilato (2 cm,
385 AD 1030-1528), Gabelotto-Fiumebianco (E-1, 218 cm, 8.4 cal ka BP), and Monte Guardia
386 (820 cm, between 22.4 ± 1.1 cal ka BP and 20.3 ± 0.7 cal ka BP). Two of them (Monte Pilato
387 and Monte Guardia) are for the first time recognized in the marine sediments of the Ionian
388 Sea, and enlarges significantly the dispersion of these tephra to the East.

389

390

391 **Acknowledgements**

392 We thank the Centre National de la Recherche Scientifique (CNRS) and Commissariat à
393 l'Energie Atomique (CEA) for basic support to the laboratory. We also thank the N/O Marion
394 Dufresne officers and crew for support and organisation of the coring cruises. BC was
395 partially supported by Vinci program of Université Franco-Italienne and SETCI from region
396 of Île-de-France. Fabien Dewilde and Elisabeth Michel (LSCE), Franco Colarieti (DST Pisa),
397 Michel Fialin and Frederic Couffignal (CAMPARIS) are gratefully acknowledged for the
398 preparation of samples and assistance during analyses. Partial funding support comes from
399 University of Pisa (Fondi di Ateneo R. Santacroce, G. Zanchetta), INGV-DPC projects
400 (Leader R. Santacroce), and SPEED-INGV project. RS acknowledge partial funding from
401 IUGG grants 2010-2011.

402

403

404

405

406 **References**

407

408 Alessio, M., Bella, F., Improta, S., Belluomini, G., Calderoni, G., Cortesi, C., Turi, F., 1974.
409 University of Rome carbon-14 dates X. *Radiocarbon*, 16: 358-367.

410

411 Arrighi, S., Tanguy, J.C., Rosi, M., 2006. Eruptions of the last 2200 years at Vulcano and
412 Vulcanello (Aeolian Islands, Italy) dated by high-accuracy archeomagnetism. *Physics of the*
413 *Earth and Planetary Interiors*, 159, 225–233. doi:10.1016/j.pepi.2006.07.010.

414

415 Aulinas, M., Civetta, L., Di Vito M.A., Orsi, G., Gimeno, D., Fèrnandes-Turiel, J.L., 2008.
416 The “pomici di mercato” Plinian eruption of Somma-Vesuvius: magma chamber processes
417 and eruption dynamics. *Bulletin of Volcanology*, 70, 825-840.

418

419 Barberi, F., Macedonio, G., Pareschi, M.T., Santacroce, R., 1990. Mapping the tephra fallout
420 risk: an example from Vesuvius, Italy. *Nature*, 344, 142-144.

421

422 Bard, E., Arnold, M., Duprat, J., Moyes, J., Duplessy, J.C., 1987. Reconstruction of the last
423 deglaciation: deconvolved records of $\delta^{18}\text{O}$ profiles, micropaleontological variations and
424 accelerator mass spectrometric ^{14}C dating. *Climate Dynamics*, 1, 101-112.

425

426 Bourne, A.J., Lowe, J.J., Trincardi, F., Asioli, A., Blockley, S.P.E., Wulf, S., Matthews, I.P.,
427 Piva, A., Vigliotti, L., 2010. Distal tephra record for the last ca 105,000 years from core
428 PRAD 1-2 in the central Adriatic Sea: implications for marine tephrostratigraphy. *Quaternary*
429 *Science Reviews*, 29 : 3079-3094.

430

431 Calanchi, N., De Rosa, R., Mazzuoli, R., Rossi, P., Santacroce, R., Ventura, G., 1993. Silicic
432 magma entering a basaltic magma chamber: eruptive dynamics and magma mixing – an
433 example from Salina (Aeolian Islands, Southern Tyrrhenian Sea). *Bulletin of Volcanology*, 55,
434 504-522.

435

436 Cioni, R., Bertagnini A., Santacroce, R., Andronico, D., 2008. Explosive activity and eruption
437 scenarios at Somma-Vesuvius (Italy): towards a new classification scheme. *Journal of*
438 *Volcanology and Geothermal Research*, 178, 331-348.

439

440 Civetta, L., Cornette, Y., Gillot, P.Y., Orsi, G., 1988. The eruptive history of Pantelleria
441 (Sicily Channel) in the last 50 ka. *Bulletin of Volcanology*, 50, 47-57.
442

443 Clift, P., Blusztajn, J., 1999. The trace-element characteristics of Aegean volcanic arc marine
444 tephra. *Journal of Volcanology and Geothermal Research*, 92, 321-347.
445

446 Costa, A., Dell'Erba, F., Di Vito, M.A., Isaia, R., Macedonio, G., Orsi, G., Pfeiffer, T., 2009.
447 Tephra fallout hazard at the Campi Flegrei caldera (Italy). *Bulletin of Volcanology*, 71, 259-
448 273.
449

450 Crisci, G.M., De Rosa, R., Lanzafame, G., Mazzuoli, R., Sheridan, M.F., Zuffa, G.G., 1981.
451 Monte Guardia sequence: a late-Pleistocene eruptive cycle on Lipari. *Bulletin of*
452 *Volcanology*, 44, 241-255.
453

454 Crisci, G.M., De Rosa, R., Esperanca, S., Mazzuoli, R., Sonnino, M., 1991. Temporal
455 evolution of a three component system: the island of Lipari (Aeolian Arc, southern Italy).
456 *Bulletin of Volcanology*, 53, 207-221.
457

458 De Astis, G., La Volpe, L., Peccerillo, A., Civetta, L., 1997. Volcanological and petrological
459 evolution of Vulcano Island (Aeolian Arc, southern Tyrrhenian Sea). *Journal of Geophysical*
460 *Research*, 102, 8021-8050.
461

462 De Rosa, R., Sheridan, M.F., 1983. Evidence for magma mixing in the surge deposits of the
463 Monte Guardia Sequence, Lipari. *Journal Volcanology Geothermal Research*, 17, 313-328.
464

465 De Rosa, R., Donato, P., Gioncada, A., Masetti, M., Santacroce, R., 2003. The Monte
466 Guardia eruption (Lipari, Aeolian Islands): an unusual example of magma mixing sequence.
467 *Bulletin of Volcanology*, 65, 530-543.
468

469 Delibrias, G., Di Paola, G.M., Rosi, M., Santacroce, R., 1979. La storia eruttiva del complesso
470 vulcanico Somma-Vesuvio ricostruita dalle successioni piroclastiche del Monte Somma.
471 *Rendiconti della Societa Italiana di Mineralogia e Petrologia*, 35: 411-438.
472
473

474 Druitt, T.H., Brenchley, P.J., Gökten, Y.E., Francaviglia, V., 1995. Late Quaternary rhyolitic
475 eruption from the Acigöl Complex, central Turkey. *Journal of Geological Society of London*,
476 152, 655–667.

477

478 Duplessy, J.C., Delibrias, G., Turon, J.L., Pujol, C., Duprat, J., 1981. Deglacial warming of
479 the northeastern Atlantic ocean: correlation with paleoclimatic evolution of the European
480 continent. *Palaeogeography, Palaeoclimatology, Palaeoecology*, 35, 121-144.

481

482 Folch, A., Sulpizio, R., 2010. Evaluating the long-range volcanic ash hazard using
483 supercomputing facilities. Application to Somma-Vesuvius (Italy), and consequences on civil
484 aviation over the Central Mediterranean Area. *Bulletin of Volcanology*, doi: 10.007/s0045-
485 010-03863.

486

487 Fontugne, M., Paterne, M., Calvert, S., Murat, A., Guichard, F., Arnold, M., 1989. Adriatic
488 deep water formation during the Holocene: implication for the reoxygenation of the deep
489 eastern Mediterranean sea. *Paleoceanography*, 4, 199-206.

490

491 Giaccio, B., Messina, P., Sposato, A., Voltaggio, M., Zanchetta, G., Galadini, F., Gori, S.,
492 Santacroce, R., 2009. Tephra layers from Holocene lake sediments of the Sulmona Basin,
493 central Italy: implications for volcanic activity in Peninsular Italy and tephrostratigraphy in
494 the central Mediterranean area. *Quaternary Science Reviews*, 28 : 2710-2733.

495

496 Juvigné, E., 1987. Deux retombées volcaniques tardiglaciaires dans le cézallier (Massif
497 Central, France). *Bulletin de l'Association Française pour l'étude du Quaternaire*, 4, 241-
498 249.

499

500 Kallel, N., Paterne, M., Labeyrie, L., Duplessy, J.C., Arnold, M., 1997. Temperature and
501 salinity records of the Tyrrhenian Sea during the last 18,000 years. *Palaeogeography*,
502 *Palaeoclimatology, Palaeoecology*, 135, 97-108.

503

504 Keller, J., Ryan, W.B.F., Ninkovich, D., Altherr, R., 1978. Explosive volcanic activity in the
505 Mediterranean over the past 200,000 yr as recorded in deep-sea sediments. *Geological Society*
506 *American Bulletin*, 89, 591–604.

507

508 Lane, C.S., Blockley, S.P.E., Lotter, A.F., Fisinger, W., Filippi, M.L. and Matthews, I.P.
509 (2010). A regional tephrostratigraphic framework for central and southern European climate
510 archives during the Last Glacial to Interglacial Transition: comparisons north and south of the
511 Alps. *Quaternary Science Reviews*, doi:10.1016/j.quascirev.2010.10.015.

512
513 Le Bas, M.J., Le Maitre, R.W., Streckeisen, A., Zanettin, B., 1986. A chemical classification
514 of volcanic rocks based on the total alkali-silica diagram. *Journal of Petrology*, 27, 745–750.
515

516 Lowe, J.J., Blockley, S., Trincardi, F., Asioli, A., Cattaneo, A., Matthews, I.P., Pollard, M.,
517 Wulf, S., 2007. Age modelling of late Quaternary marine sequences in the Adriatic: towards
518 improved precision and accuracy using volcanic event stratigraphy. *Continental Shelf*
519 *Research*, 27, 560–582.

520

521 Margari, V., Pyle, D.M, Brynt, C., Gibbart, P.L., 2007. Mediterranean tephrostratigraphy
522 revisited: results from a long terrestrial sequence on Lesbos Island, Greece. *Journal of*
523 *Volcanology and Geothermal Research*, 163, 34-54.

524

525 McCoy, F.W. 1981. Areal distribution, redeposition and mixing of tephra within deep-sea
526 sediments of the Eastern Mediterranean Sea. In *Self, S and Sparks, RSJ (Editors), Tephra*
527 *Studies. Reidel Dordrecht*, 245-254.

528

529 Mele D., Sulpizio R., Dellino P., La Volpe L., 2010. Stratigraphy and eruptive dynamics of a
530 long-lasting Plinian eruption of Somma-Vesuvius: the Pomici di Mercato (8900 years BP).
531 *Bulletin of Volcanology*, doi 10.007/S00445-010-0407-2.

532

533 Mercone, D., Thomson, J., Croudace, I.W., Siani, G., Paterne, M., Tröelstra, S., 2000.
534 Duration of S1, the most recent Eastern Mediterranean sapropel, as indicated by AMS
535 radiocarbon and geochemical evidence. *Paleoceanography*, 15, 336-347.
536

537 Narcisi, B., 2002. Tephrostratigraphy of the Late Quaternary lacustrine sediments of Lago di
538 Pergusa (central Sicily). *Bollettino Società Geologica Italiana*, 121, 211-219.
539

540 Paterne, M., Guichard, F., Labeyrie, J., Gillot, P.Y., Duplessy, J.C., 1986. Tyrrhenian Sea
541 tephrochronology of the oxygen isotope record for the past 60,000 years. *Marine Geology*,
542 72, 259-285.

543

544 Paterne, M., Guichard, F., Labeyrie, J., 1988. Explosive activity of the South Italian
545 volcanoes during the past 80,000 years as determined by marine tephrochronology. *Journal*
546 *of Volcanology Geothermal Research*, 34, 153-172.

547

548 Paterne, M., Labeyrie, J., Guichard, F., Massaud, A., Maitre, F., 1990. Fluctuation of the
549 campanian explosive activity (South Italy) during the last 190,000 years as determined by
550 marine tephrochronology. *Earth and Planetary Science Letters*, 98, 166-174.

551

552 Paterne, M., Guichard, F., Duplessy, J.C., Siani, G., Sul pizio, R., Labeyrie, J., 2008. A
553 90,000 – 200,000 yrs marine tephra record of Italian volcanic activity in the central
554 Mediterranean Sea. *Journal of Volcanology and Geothermal Research*, 177, 187–196.

555

556 Reimer, P.J., Baillie, M.G.L., Bard, E., Bayliss, A., Beck, J.W., Blackwell, P.G., Bronk
557 Ramsey, C., Buck, C.E., Burr, G.S., Edwards, R.L., Friedrich, M., Grootes, P.M., Guilderson,
558 T.P., Hajdas, I., Heaton, T.J., Hogg, A.G., Hughen, K.A., Kaiser, K.F., Kromer, B.,
559 McCormac, F.G., Manning, S.W., Reimer, R.W., Richards, D.A., Southon, J.R., Talamo, S.,
560 Turney, C.S.M., van der Plicht, J. and Weyhenmeyer, C.E. (2009) INTCAL 09 and
561 MARINE09 radiocarbon age calibration curves, 0-50,000 years Cal BP. *Radiocarbon*, 51:
562 1111-1150. ISSN 0033-8222.

563

564 Rohling, E.J., Jorissen, F.J., De Stigter, H.C., 1997. 200 year interruption of Holocene
565 sapropel formation in the Adriatic sea. *Journal of Micropaleontology*, 16, 97-108.

566

567 Santacroce, R., (ed.) 1987. Somma-Vesuvius. *Quaderni la Ricerca, Scientifica*, 114, 200 pp.

568

569 Santacroce, R. and Sbrana, A., 2003. Geological map of Somma-Vesuvius, scale 1:15000.
570 *Selca, Firenze*.

571

572 Santacroce, R., Cioni, R., Marianelli, P., Sbrana, A., Sul pizio, R., Zanchetta, G., Donahue,
573 D.J., Joron, J.L., 2008. Age and whole rock-glass compositions of proximal pyroclastics from

574 the major explosive eruptions of Somma-Vesuvius: a review as a tool for distal
575 tephrostratigraphy. *Journal of Volcanology and Geothermal Research*, 177, 1–18.
576

577 Siani, G., Paterne, M., Arnold, M., Bard, E., Métiévier, B., Tisnerat, N., Bassinot, F., 2000.
578 Radiocarbon reservoir ages in the Mediterranean Sea and Black Sea coastal waters.
579 *Radiocarbon*, 42 (2), 271–280.
580

581 Siani, G., Paterne, M., Michel, E., Sulpizio, R., Sbrana, A., Arnold, M., Haddad, G., 2001.
582 Mediterranean sea-surface radiocarbon reservoir age changes since the last glacial maximum.
583 *Science*, 294, 1917-1920.
584

585 Siani, G., Sulpizio, R., Paterne, M., Sbrana, A., 2004. Tephrostratigraphy study for the last
586 18,000 ¹⁴C years in a deep-sea sediment sequence for the South Adriatic. *Quaternary Science*
587 *Reviews*, 23, 2485-2500.
588

589 Siani G., Paterne, M., Colin, C. (2010) - Late Glacial to Holocene planktic foraminifera
590 bioevents and climatic record in the South Adriatic Sea. *Journal of Quaternary Science*, 25:
591 808-821.
592

593 Stuiver, M., Reimer, P.J., Bard, E., Beck, J.W., Burr, G.S., Hughen, K.A., Kromer, B.,
594 McCormac, G., van der Plicht, J., Spurk, M., 1998. INTCAL98 radiocarbon age calibration,
595 24000-0 cal BP. *Radiocarbon*, 40, 1041–1083.
596

597 Sulpizio, R., Bonasia, L., Dellino, P., La Volpe, P., Mele, Zanchetta, G., Di Vito, M.A.,
598 Sadori, L., 2008. Discriminating the long distance dispersal of fine ash from sustained
599 columns or near ground ash clouds: the example of the Avellino eruption (Somma-Vesuvius,
600 Italy). *Journal of Volcanology and Geothermal Research*, 177, 263-276.
601

602 Sulpizio, R., Cioni, R., Di Vito, M.A., Mele, D., Bonasia, R., Dellino, P., 2010. The Pomice di
603 Avellino eruption of Somma-Vesuvius (3.9 ka BP) part I: stratigraphy, compositional
604 variability and eruptive dynamics. *Bulletin of Volcanology*, 72, 539-558, DOI
605 10.1007/s00445-009-0339-x.
606

607 Thunell, R., Federman, A., Sparks, S., Williams, D., 1979. The age, origin, and
608 volcanological significance of the Y-5 ash layer in the Mediterranean. *Quaternary Research*,
609 12, 241-253.

610

611 Turney, C.S.M., Blockley, S.P.E., Lowe, J.J., Wulf, S., Branch, N.P., Mastrolorenzo, G.,
612 Swindle, G., Nathan, R., Pollard, A.M., 2008. Geochemical characterization of Quaternary
613 tephras from the Campanian province. Italy. *Quaternary International*, 178, 288–305.

614

615 Vogel, H., Zanchetta, G., Sulpizio, R., Wagner, B., Nowaczyk, N., 2010. A
616 tephrostratigraphic record for the last glacial-interglacial cycle from Lake Ohrid, Albania and
617 Macedonia. *Journal of Quaternary Science*, 25, 320-338.

618

619 Wulf, S., Kraml, M., Brauer, A., Keller, J., Negendank, J.F.W., 2004. Tephrochronology of
620 the 100 ka lacustrine sediment record of Lago Grande di Monticchio (southern Italy).
621 *Quaternary International*, 122, 7–30.

622

623 Wulf, S., Kraml, M., Keller, J., 2008. Towards a detailed distal tephrostratigraphy in the
624 Central Mediterranean: the last 20,000 yrs record of Lago Grande di Monticchio. *Journal of*
625 *Volcanology and Geothermal Research*, 177, 118–132.

626

627 Zanchetta, G., Di Vito, M., Fallick, A.E., Sulpizio, R., 2000. Stable isotopes of pedogenic
628 carbonate from Somma-Vesuvius area, southern Italy, over the last 18 ka: palaeoclimatic
629 implications. *Journal of Quaternary Science*, 15 (8), 813-824.

630

631 Zanchetta, G., Sulpizio, R., Roberts, N., Cioni, R., Eastwood, W.J., Siani, G., Caron, B.,
632 Paterne, M., Santacroce, R., 2011. Tephrostratigraphy, chronology and climatic events of the
633 Mediterranean basin during the Holocene: an overview. *The Holocene*, 21: 33-52, doi:
634 10.1177/09596683610377531.

635

636 Zanella, E., 2006. Magnetic chronology in recent volcanic rocks: basic principles and case
637 histories from Aeolian Islands. *Acta Vulcanologica*, 18 (1-2), 35-46.

638

639 **Figure and Table captions**

640

641 **Figure 1:** Location map of the study area, of the main Italian volcanoes and location of cores
642 used in this study. CVZ = Campanian Volcanic Zone (Campi Flegrei, Somma-Vesuvius,
643 Ischia and Procida), AI = Aeolian Islands, LGM = Lago Grande di Monticchio, LdP = Lago
644 di Pergusa.

645

646 **Figure 2:** Lithostratigraphy, AMS ^{14}C dates (crosses), variations in $\delta^{18}\text{O}$ (per mil) of
647 *Globigerina bulloides*, glass shards abundance curve, mass magnetic susceptibility and age
648 model of the deep sea core MD 90-918.

649

650 **Figure 3:** General TAS diagram with geochemical compositions of the marine tephra layers
651 from core MD 90-918 (Le Bas et al., 1986).

652

653 **Figure 4:** Stratigraphy details of the relative abundance and composition of glass shards
654 during the Sapropel S1 in core MD 90-918.

655

656 **Figure 5:** SEM pictures of volcanic glass fragments from tephra layer a) 2 cm, b) 175 cm, c)
657 185 cm, d) 210 cm, e) 218 cm, f) 223 cm, g) 230 cm and h) 820 cm.

658

659

660 **Figure 6:** Comparison of the geochemical compositions of the ash-layers in core MD 90-918
661 with those on the continental and marine deposits from the literature plotted in TAS diagram:
662 a) Monte Pilato eruption ca. AD 1200, samples PI 134 from Lipari Island and correlation with
663 the tephra layer at 2-5 cm; c) Mercato eruption samples from the Somma-Vesuvius (Wulf et
664 al., 2004; Santacroce et al., 2008; Turney et al., 2008 and Paterne et al., 1988) and correlation
665 with the tephra layers at 230, 223, 210, 185 and 175 cm; d) Gabelotto-Fiumebianco eruption
666 and E-1 tephra layer samples from the Lipari Island (Siani et al., 2004; Paterne et al., 1988)
667 and correlation with the tephra layer at 218 cm; e) Monte Guardia eruption samples from the
668 Lipari Island (De Rosa et al., 2003) and correlation with the tephra layers at 820 cm.

669

670 **Figure 7:** Map of the ash dispersion for a) Monte Pilato ca. AD 1200 from Lipari Island, b)
671 Mercato eruption from the Somma-Vesuvius, c) Gabelotto-Fiumebianco eruption from Lipari
672 Island and d) Monte Guardia eruption from Lipari. Stars indicate the volcanic sources.

673

674 **Table 1:** Intercalibration data between SEM-DST (University of Pisa, Italy) and the EPMA-
675 CAMPARIS (University of Pierre et Marie Curie of Paris, France). A set of 99 analyses of
676 five distinct tephra layers is resumed here with: 1) the mean of all analyses from the two
677 instruments; 2) the mean of the analyses from the both instrument; 3) the difference between
678 the means of the analyses from the two instruments; 4) the standard deviation of the means of
679 the analyses from the two instruments; 5) the variance in % of the means of analyses from the
680 two instruments; 6) and finally the average of variance of the distinct layers.

681

682 **Table 2:** Conventional ^{14}C ages from MD 90-918 core determined by UMS-ARTEMIS
683 (Pelletron 3MV) AMS facilities (CNRS-CEA Gif-sur-Yvette, France). The conventional
684 radiocarbon ages were converted into calendar ages, based on INTCAL09 (Reimer et al.,
685 2009) using the ^{14}C calibration software CALIB 6 (Stuiver et al., 1998). The calibration
686 integrate a marine reservoir correction $R(t)$ of about 400 years (Siani et al., 2000).

687

688 **Table 3:** Composition of major elements analyses of the eight tephra layers recognized in
689 core MD 90-918. Analyses performed on the SEM-DST (University of Pisa, Italy) and the
690 EPMA-CAMPARIS (University of Pierre et Marie Curie of Paris, France).

691

692 **Table 4:** Average and standard deviation of analyses from literature used for comparison
693 except the analyses from PI-134 which is a sample collected on the cone Monte Pilato
694 eruptive succession from the Lipari Island.

695

Figure 1
[Click here to download high resolution image](#)

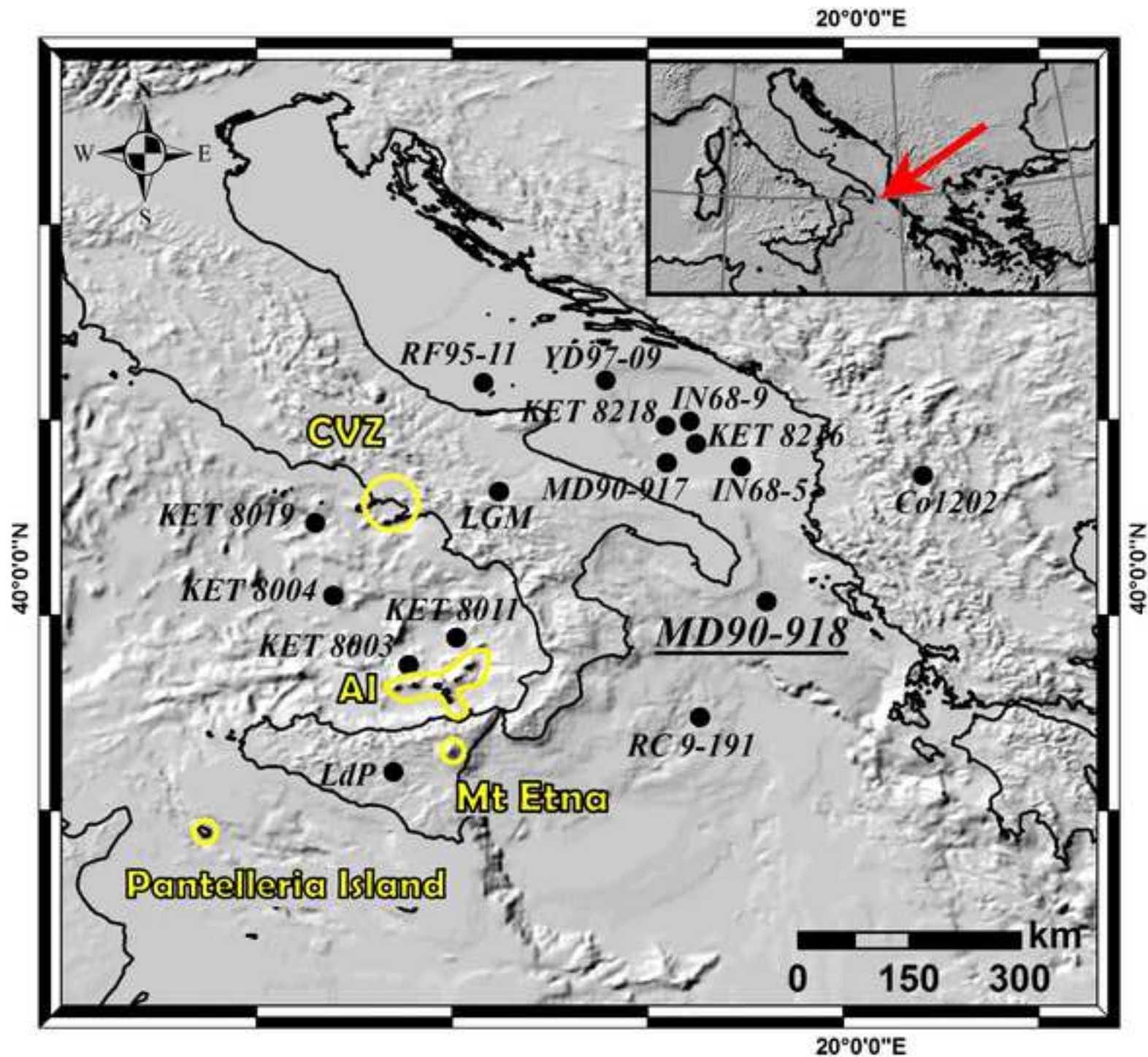


Figure 2
[Click here to download high resolution image](#)

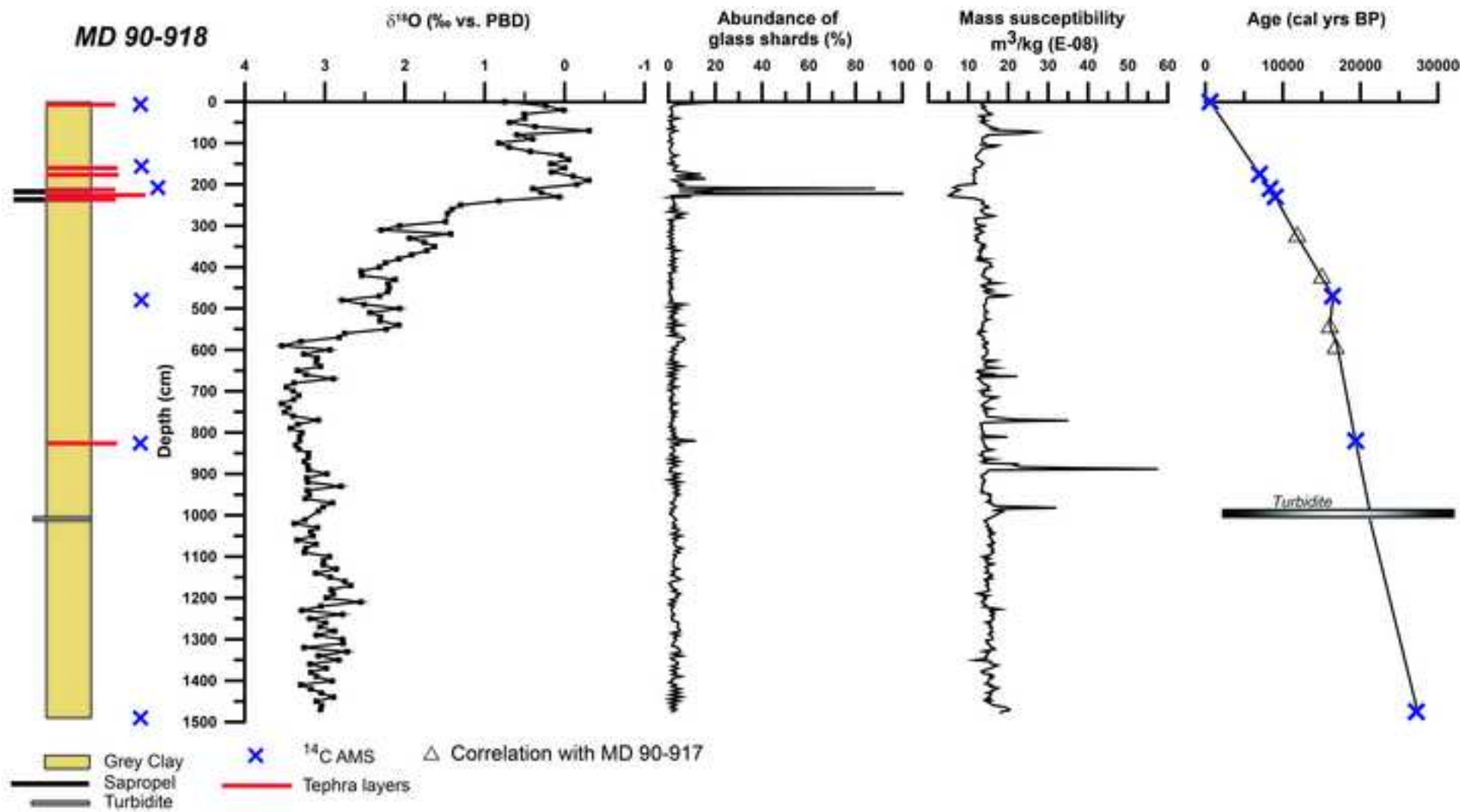


Figure 3

[Click here to download high resolution image](#)

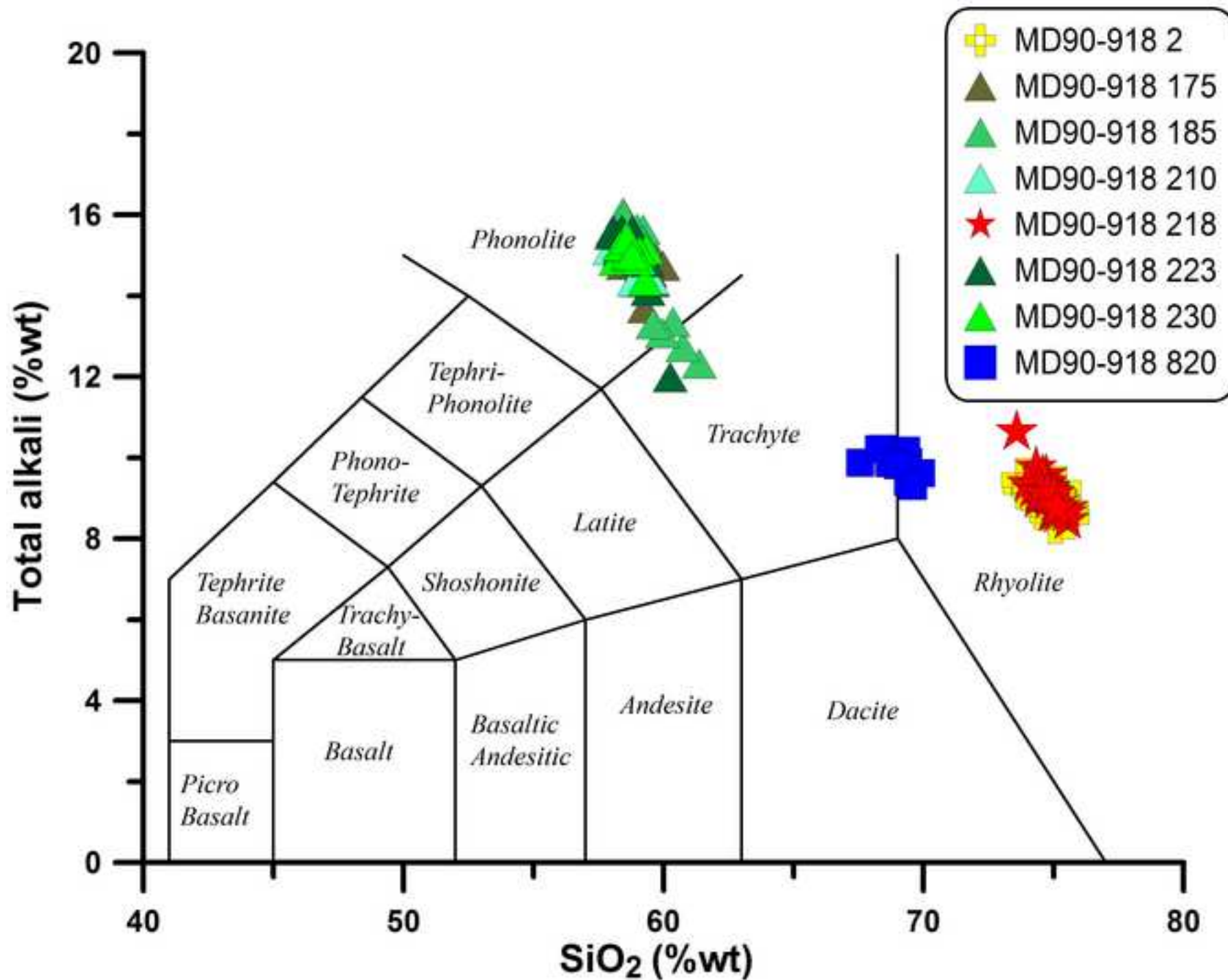


Figure 4
[Click here to download high resolution image](#)

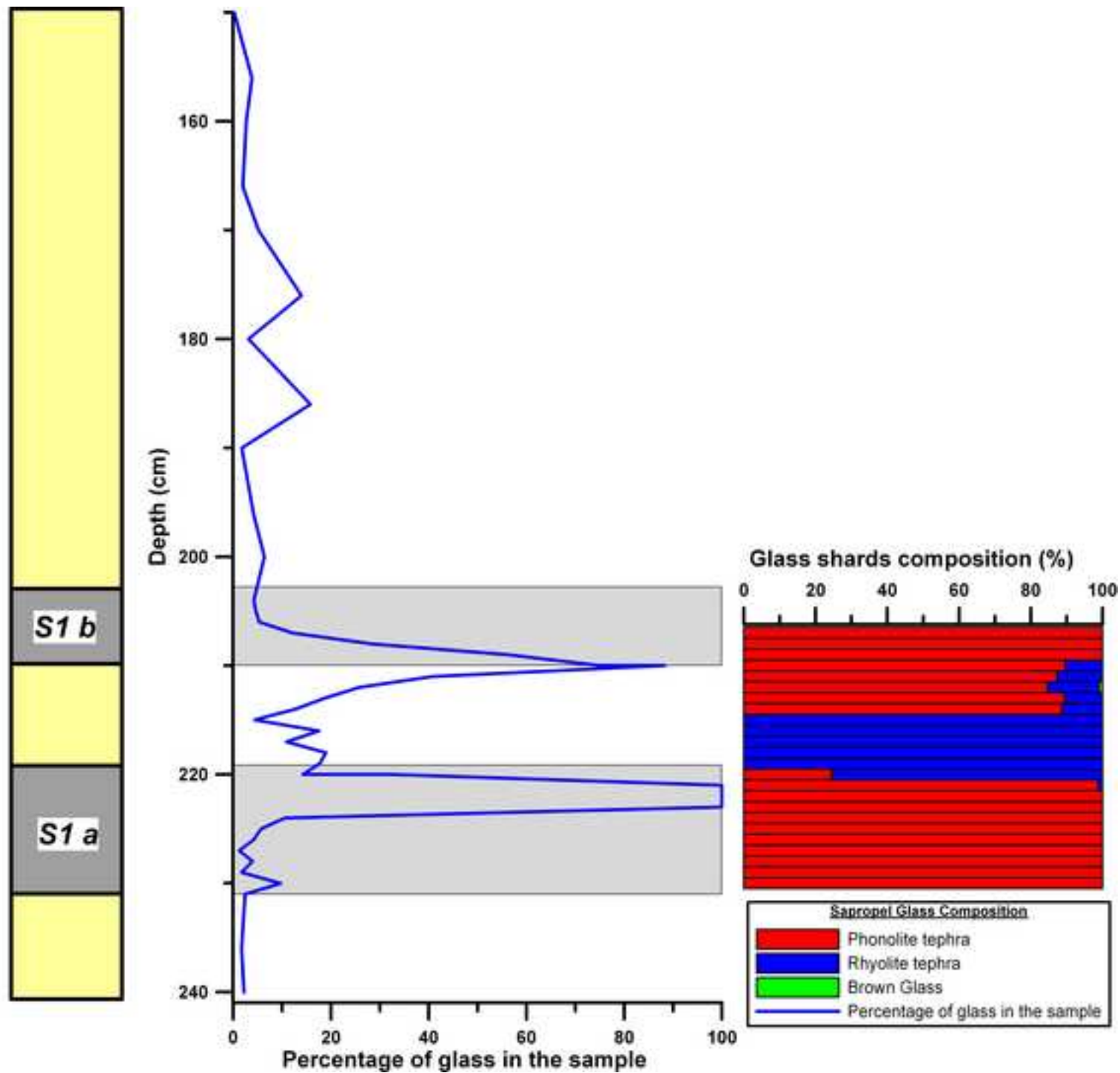


Figure 5
[Click here to download high resolution image](#)

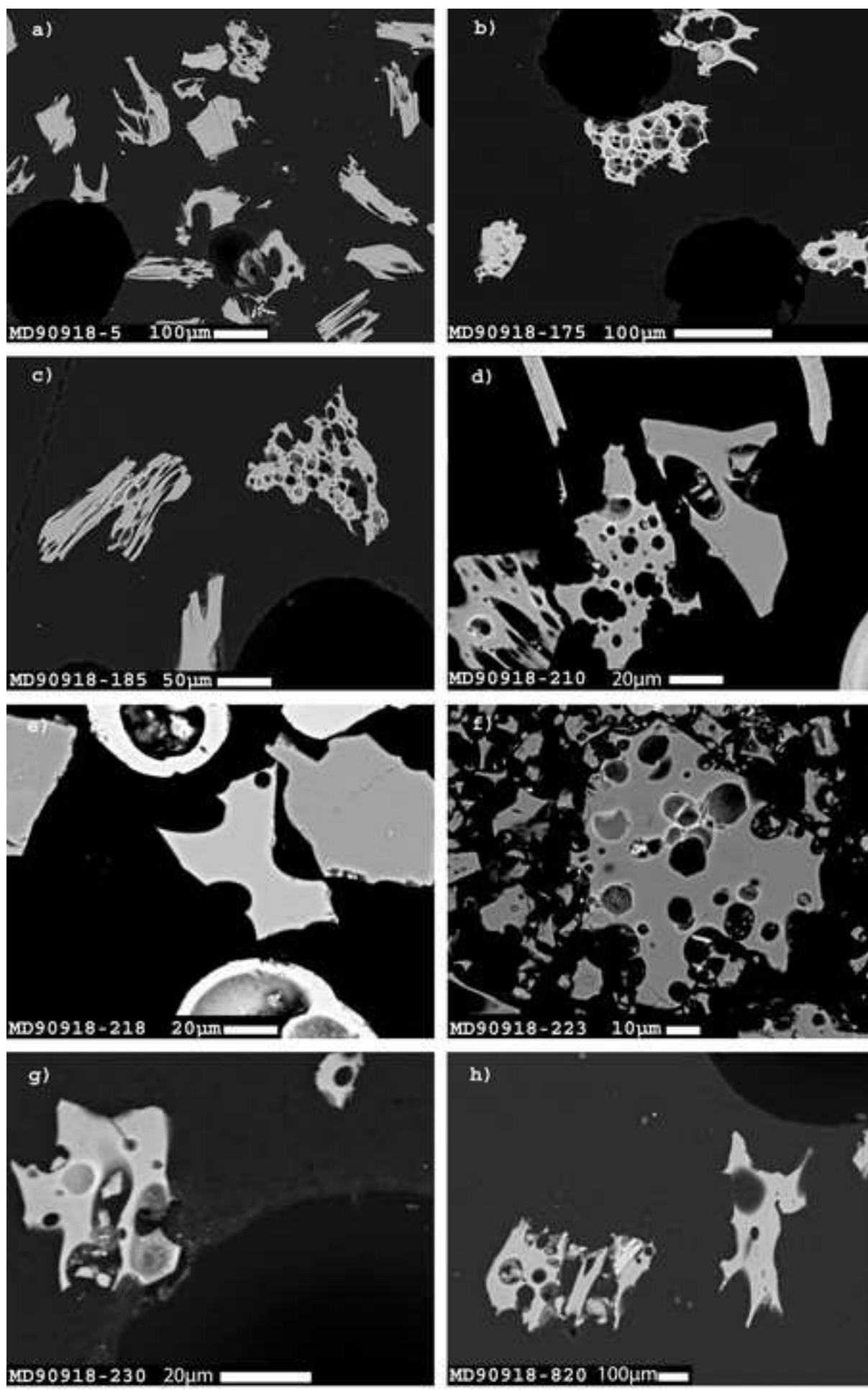


Figure 6

[Click here to download high resolution image](#)

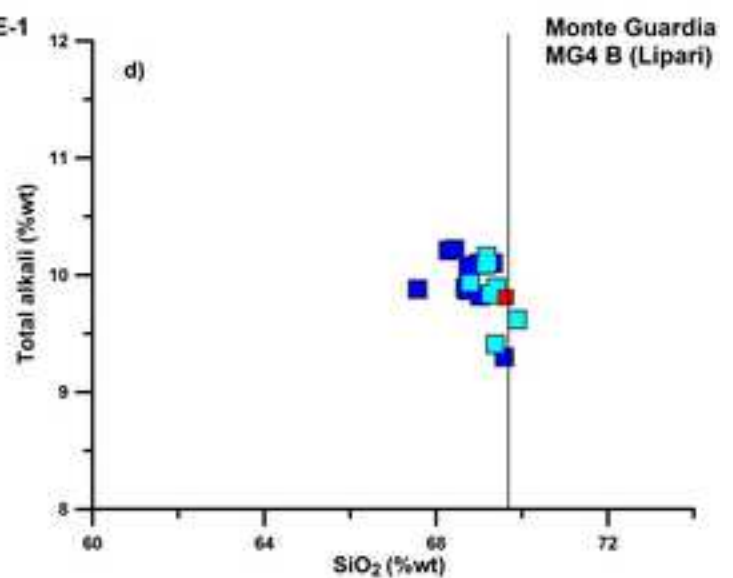
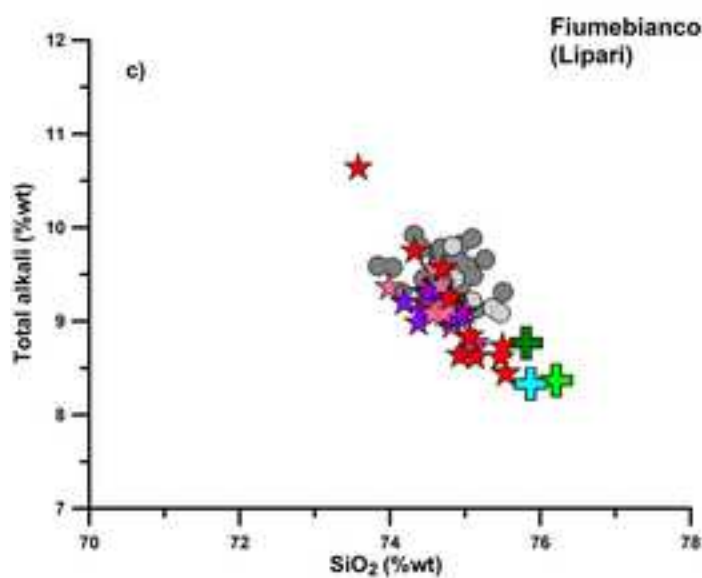
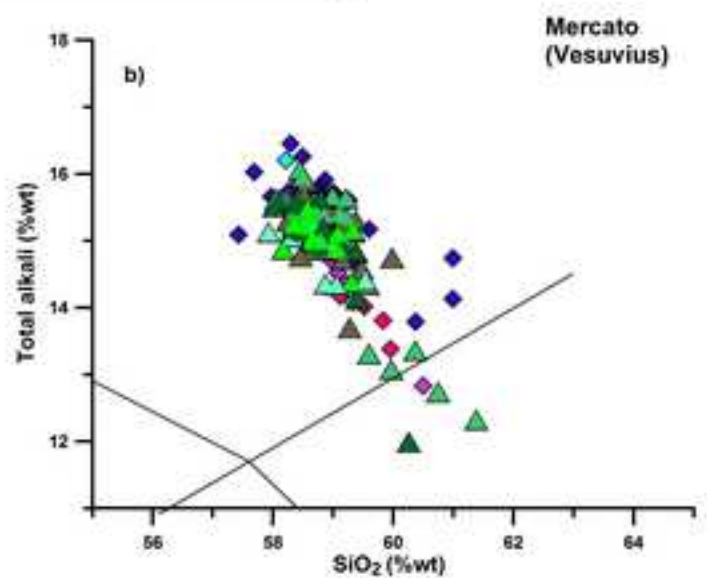
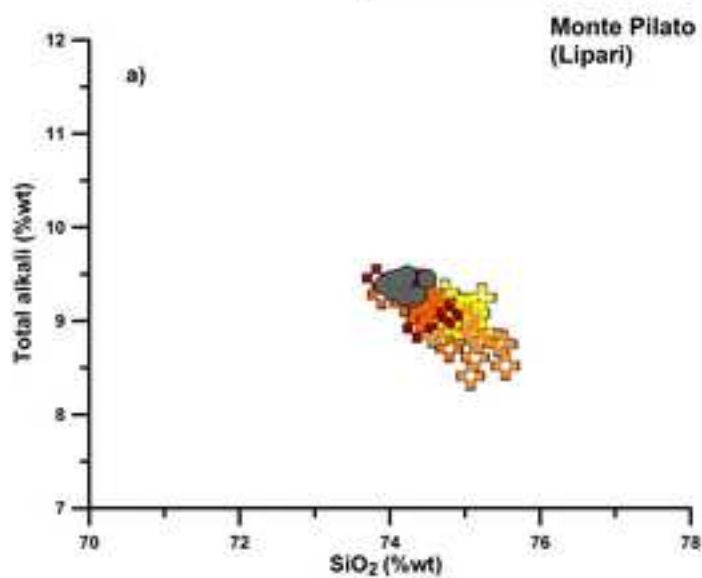
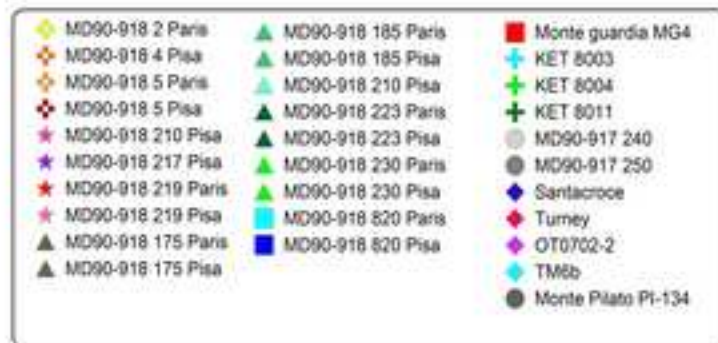


Figure 7
[Click here to download high resolution image](#)

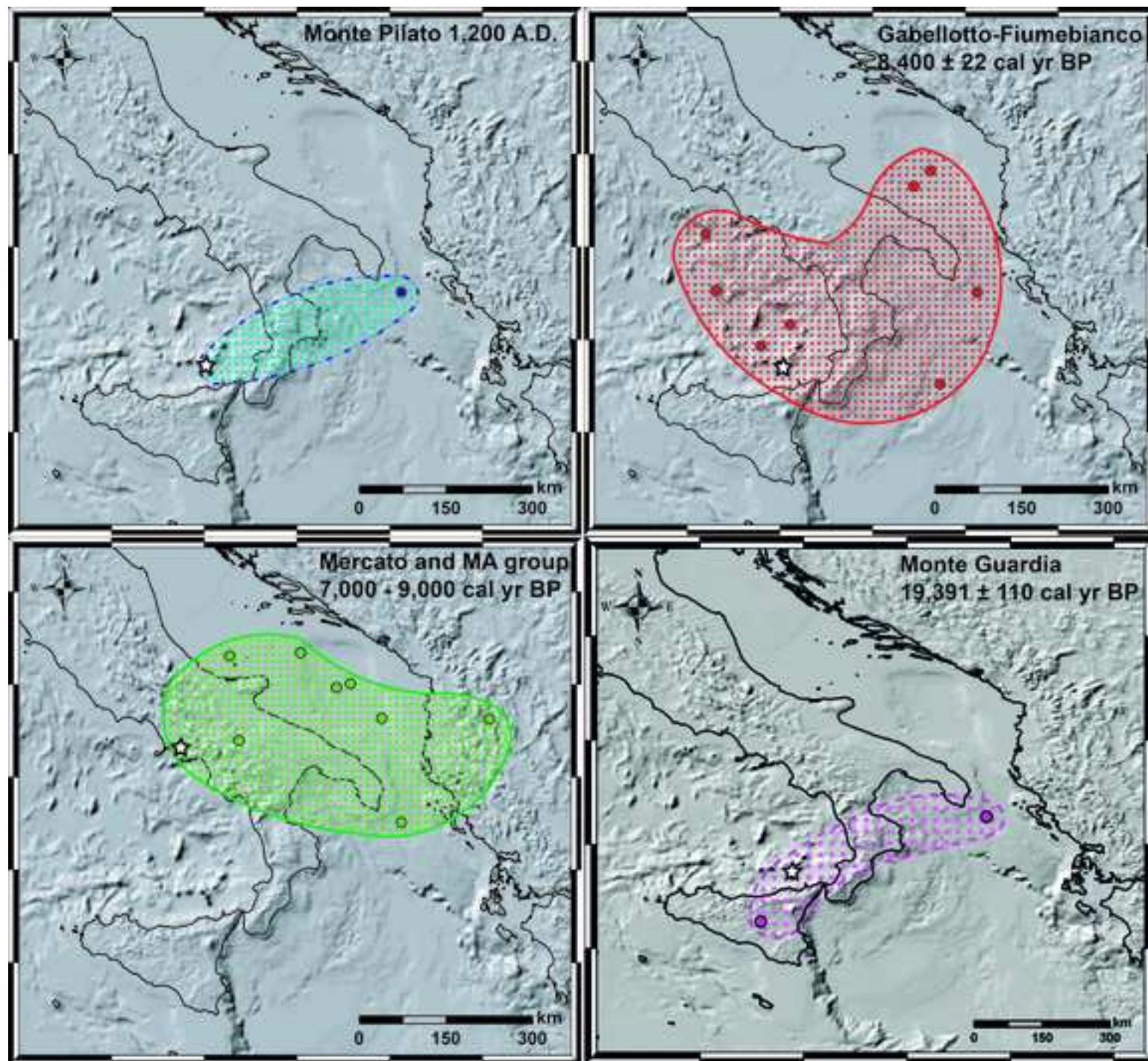


Table 1

[Click here to download Table: Table1_EDS-microsonde.xls](#)

	SiO ₂	TiO ₂	Al ₂ O ₃	FeO _{tot}	MnO	CaO	Na ₂ O	K ₂ O	ClO	
Level 5	Mean of all analyses from the level 5	74.81	0.05	13.41	1.51	0.05	0.78	4.02	4.95	0.37
	Mean from the EPMA-CAMPARIS analyses	75.18	0.06	13.22	1.52	0.07	0.79	3.98	4.76	0.38
	Mean from the SEM-DST analyses	74.44	0.05	13.61	1.49	0.03	0.78	4.05	5.14	0.36
	Difference between the two means	0.74	0.01	-0.39	0.03	0.04	0.01	-0.07	-0.38	0.02
	Sd of the two means	0.52	0.01	0.27	0.02	0.03	0.00	0.05	0.27	0.01
	% variance of the two means from both instrument	0.98	15.42	2.91	2.06	59.28	0.70	1.88	7.95	4.58
Level 175	Mean of all analyses from the level 175	58.92	0.14	21.53	1.72	0.20	1.65	8.45	6.71	0.57
	Mean from the EPMA-CAMPARIS analyses	59.01	0.15	21.28	1.71	0.20	1.68	8.58	6.69	0.59
	Mean from the SEM-DST analyses	58.79	0.13	21.87	1.74	0.19	1.60	8.28	6.73	0.55
	Difference between the two means	0.22	0.03	-0.59	-0.03	0.01	0.08	0.30	-0.05	0.05
	Sd of the two means	0.16	0.02	0.42	0.02	0.01	0.05	0.21	0.03	0.03
	% variance of the two means from both instrument	0.38	16.87	2.77	1.49	6.51	4.62	3.46	0.70	7.86
Level 185	Mean of all analyses from the level 185	58.74	0.15	21.43	1.69	0.18	1.59	8.86	6.65	0.59
	Mean from the EPMA-CAMPARIS analyses	58.91	0.16	21.19	1.68	0.18	1.61	8.90	6.64	0.64
	Mean from the SEM-DST analyses	58.48	0.15	21.80	1.72	0.19	1.56	8.78	6.65	0.51
	Difference between the two means	0.43	0.01	-0.61	-0.04	-0.01	0.06	0.12	0.00	0.14
	Sd of the two means	0.30	0.01	0.43	0.03	0.01	0.04	0.08	0.00	0.10
	% variance of the two means from both instrument	0.73	4.94	2.90	2.46	4.79	3.57	1.35	0.07	21.23
Level 219	Mean of all analyses from the level 219	74.80	0.07	13.21	1.48	0.07	0.84	3.92	5.20	0.34
	Mean from the EPMA-CAMPARIS analyses	74.95	0.07	13.08	1.50	0.07	0.84	3.91	5.16	0.37
	Mean from the SEM-DST analyses	74.58	0.07	13.40	1.46	0.06	0.83	3.95	5.28	0.31
	Difference between the two means	-0.37	0.00	0.31	-0.04	-0.01	-0.01	0.04	0.13	-0.07
	Sd of the two means	0.26	0.00	0.22	0.03	0.01	0.01	0.03	0.09	0.05
	% variance of the two means from both instrument	0.49	5.93	2.37	2.90	11.86	1.29	1.01	2.43	18.15
Level 820	Mean of all analyses from the level 820	68.97	0.30	16.08	2.27	0.13	1.49	4.57	5.36	0.33
	Mean from the EPMA-CAMPARIS analyses	69.31	0.27	15.79	2.29	0.13	1.50	4.59	5.29	0.32
	Mean from the SEM-DST analyses	68.74	0.32	16.27	2.27	0.13	1.48	4.56	5.40	0.33
	Difference between the two means	0.57	-0.05	-0.48	0.02	0.01	0.02	0.03	-0.11	-0.01
	Sd of the two means	0.40	0.04	0.34	0.02	0.00	0.02	0.02	0.08	0.00
	% variance of the two means from both instrument	0.82	20.18	3.03	1.05	5.11	1.61	0.68	2.07	1.82
average of the % variance		0.68	12.67	2.80	1.99	17.51	2.36	1.68	2.65	10.73

nb=99

Table 2

[Click here to download Table: Table2_foram_14C.xls](#)

Laboratory Number	Core Depth (cm)	Species	¹⁴ C AMS age (yr BP)	± Error (yr)	Calibrated yr BP (range 1σ)	Source
SacA 15142	0-6	<i>G. ruber</i>	960	35	601-629	<i>intcal09</i>
SacA 15143	175-177	<i>G. ruber</i>	6535	45	6949-7029	<i>intcal09</i>
SacA 18291	215-217	<i>G. ruber</i>	7810	45	8237-8310	<i>intcal09</i>
SacA 15148	230-232	<i>G. ruber</i>	8470	50	8975-9034	<i>intcal09</i>
	300				11660	<i>Siani et al. 2010</i>
	420				14840	<i>Siani et al. 2010</i>
SacA 15149	470-472	<i>G. bulloides</i>	13740	60	16266-16724	<i>intcal09</i>
	590				17000	<i>Siani et al. 2010</i>
SacA 15150	820-822	<i>G. bulloides</i>	16610	70	19260-19465	<i>intcal09</i>
SacA 15151	1475-1477	<i>G. bulloides</i>	22710	110	27267-27513	<i>intcal09</i>

Table 3

[Click here to download Table: table3_MD90-918.xls](#)

MD90-918 2-Paris	SiO₂	TiO₂	Al₂O₃	FeO_{tot}	MnO	MgO	CaO	Na₂O	K₂O	P₂O₅	ClO	Total	Total Alkali	K₂O/Na₂O
3/1.	75.14	0.09	13.14	1.27	0.03	0.05	0.79	4.09	4.99	0.00	0.39	100	9.08	1.22
5/1.	75.02	0.14	13.02	1.37	0.06	0.06	0.81	3.81	5.33	0.02	0.36	100	9.15	1.40
6/1.	75.23	0.00	12.88	1.49	0.10	0.04	0.67	3.83	5.42	0.02	0.32	100	9.25	1.41
7/1.	75.09	0.21	12.95	1.51	0.04	0.04	0.76	3.88	5.12	0.00	0.40	100	9.01	1.32
8/1.	74.57	0.01	13.40	1.46	0.13	0.03	0.87	3.90	5.22	0.03	0.37	100	9.12	1.34
9/1.	74.93	0.00	13.07	1.61	0.06	0.05	0.78	3.96	5.18	0.02	0.33	100	9.15	1.31
10/1.	75.03	0.00	13.07	1.63	0.07	0.05	0.74	4.01	5.04	0.00	0.36	100	9.06	1.26
11/1.	74.73	0.27	13.06	1.39	0.07	0.04	0.76	3.82	5.48	0.00	0.37	100	9.30	1.43
12/1.	75.21	0.05	13.09	1.49	0.12	0.04	0.75	3.98	4.89	0.00	0.37	100	8.88	1.23
14/1.	74.73	0.01	13.49	1.62	0.06	0.05	0.77	4.02	4.87	0.02	0.37	100	8.89	1.21
16/1.	74.90	0.02	13.23	1.54	0.11	0.05	0.81	3.73	5.21	0.00	0.40	100	8.94	1.40
17/1.	74.78	0.15	13.26	1.53	0.09	0.04	0.78	3.83	5.15	0.03	0.36	100	8.98	1.34
18/1.	74.69	0.01	13.27	1.58	0.06	0.05	0.77	3.97	5.21	0.01	0.38	100	9.19	1.31
19/1.	75.00	0.02	13.14	1.57	0.05	0.05	0.75	3.90	5.07	0.04	0.39	100	8.98	1.30
mean	74.93	0.07	13.15	1.50	0.07	0.05	0.77	3.91	5.16	0.01	0.37	-	9.07	1.32
sd	0.21	0.09	0.17	0.11	0.03	0.01	0.05	0.10	0.18	0.01	0.02	-	0.13	0.07
MD90-918 4-Pisa	SiO₂	TiO₂	Al₂O₃	Fe₂O₃	MnO	MgO	CaO	Na₂O	K₂O	P₂O₅	ClO	Total	Total Alkali	K₂O/Na₂O
PI151-1	74.51	0.00	13.63	1.51	0.00	0.14	0.75	3.95	5.25	0.00	0.27	100	9.20	1.33
PI151-2	74.56	0.00	13.44	1.53	0.00	0.09	0.85	3.93	5.26	0.00	0.33	100	9.19	1.34
PI151-3	74.55	0.00	13.52	1.48	0.00	0.00	0.88	3.98	5.30	0.00	0.29	100	9.28	1.33
PI151-4	73.89	0.00	14.18	1.37	0.00	0.08	0.89	4.21	5.07	0.00	0.26	100	9.28	1.20
PI151-5	74.41	0.23	13.44	1.55	0.19	0.05	0.78	3.76	5.26	0.00	0.34	100	9.02	1.40
PI151-6	74.44	0.11	13.44	1.68	0.00	0.07	0.79	3.80	5.30	0.00	0.36	100	9.10	1.39
PI151-7	74.79	0.07	13.65	1.57	0.00	0.08	0.72	3.68	5.03	0.00	0.42	100	8.71	1.37
PI151-8	74.48	0.00	13.46	1.46	0.00	0.09	0.85	4.01	5.23	0.00	0.43	100	9.24	1.30
PI151-9	74.19	0.09	13.60	1.53	0.06	0.20	0.82	3.92	5.28	0.00	0.30	100	9.20	1.35
PI151-10	74.42	0.00	13.55	1.45	0.00	0.08	0.78	3.85	5.49	0.00	0.37	100	9.34	1.43
mean	74.42	0.05	13.59	1.51	0.03	0.09	0.81	3.91	5.25	0.00	0.34	-	9.16	1.34
sd	0.24	0.08	0.22	0.08	0.06	0.05	0.06	0.15	0.13	0.00	0.06	-	0.18	0.06

